Anisotropy in MgO Measured in the Deformation-DIA by using High-resolution Monochromatic Diffraction

T. Uchida, Y. Wang, M.L. Rivers, S.R. Sutton
Consortium for Advanced Radiation Sources, The University of Chicago, Chicago, IL, U.S.A.

Introduction

Crystalline materials are generally elastically anisotropic. Even cubic materials are characterized by three elastic constants, whereas isotropic elastic material has only two. To define elastic anisotropy for the cubic materials, it is common to use the elastic anisotropy factor $S = S_{11}-S_{12}-S_{44}/2$ or $A = 2(S_{11}-S_{12})/S_{44}$, where S_{ij} are elastic compliances. Materials become isotropic when $S = 0$ or $A = 1$. Recent high-pressure ultrasonic and Brillouin scattering experiments show that elastic anisotropy in MgO (fcc) remains positive, decreasing only modestly with pressure. If we extrapolate the anisotropy reported in these measurements to higher pressures, S becomes zero at a pressure of 11 GPa [1], 19 GPa [2], 21 GPa [3], and 21.5 GPa [4]. On the other hand, diffraction studies in the Drickamer cell [5] show that MgO becomes elastically isotropic at much lower pressures between 2 and 4 GPa.

To address the discrepancy in the anisotropy factor between diffraction observations and ultrasonic or Brillouin scattering data, we examined nonhydrostatic strain in MgO up to 6 GPa at room temperature by using deformation-DIA (D-DIA) [6] and monochromatic diffraction with a 2-D charge-coupled device (CCD) detector. We used sintered polycrystalline cubic boron nitride (cBN) anvils that are x-ray transparent, which enabled us to collect complete Debye rings (with the entire 360° azimuth coverage) with a 2θ range up to about 12°. By using high-energy x-rays (small wavelengths), diffraction lines down to about 1 Å can be recorded within this 2θ range. The ellipticity of the Debye rings provided information on elastic lattice strains due to the differential stress. An iso-stress (Reuss) model was assumed, and anisotropy A was estimated from the lattice strains. The correlation between anisotropy and the differential stress level is discussed here.

Methods and Materials

Experimental details are described by Uchida et al. [7]. Two experiments were conducted, both with two deformation cycles at two different pressures. In the first run, pressure was increased to 2 GPa, and the differential rams were advanced by 0.4 mm in total displacement (0.2 mm for each ram). The pressure was then increased to 6 GPa, where the differential rams were advanced by another 0.5 mm. Finally the ram load was released. In the second run, pressure was first increased to 5 GPa, and both rams were advanced by 0.35 mm. Then the pressure was decreased to 1.5 GPa, followed by another 0.4-mm ram advancement, after which the main ram load was released.

Results and Discussion

Figure 1 compares lattice strains of all three peaks — *111*, *200*, and *220* (italics denote crystal plane) — as a function of the azimuth angle φ. The scattering in the *111* lattice distortion is mainly due to the low intensity of this peak; hence, the autofitting routine was unable to determine the peak center at certain azimuth angles. However, even for this low-intensity peak, the majority of the data are quite robust. At 2 GPa, it is clear that the lattice strain for *200* is significantly greater than that for *220*, while at 6 GPa, lattice strains for *200* and *220* are identical. We observed identical behavior in both runs. The systematic difference in lattice strains between the *200* and *220* peaks is interpreted as the anisotropy factor S (positive) being close to zero at around 6 GPa, since over a large range of overall displacement with various pressure and ram advancement histories, lattice strains are consistently anisotropic at low pressures (1.5-2 GPa) and isotropic at high pressures (5-6 GPa). Duffy et al. [8] and Uchida et al. [5] observed the same feature in the diamond anvil cell (DAC) and Drickamer cell, respectively, with a slight variation in pressure observed when the d-spacings of the *200* and *220* reflections were compared. Merkel et al. [9] also reported a consistent anisotropy change around 8 GPa.

In lattice strain theory [10], both $S = 0$ (material becomes elastically isotropic) and $\alpha = 0$ (polycrystalline packing approaches iso-strain [Voigt] limit) result in identical strains $\varepsilon(\varphi, hkl)$ for all Miller indices *hkl*, where the parameter α denotes the boundary condition at grain contacts and has a value between 0 (iso-strain) and 1 (iso-stress). These two situations can be distinguished by examining the strong correlation between anisotropy factor S and the systematic differences in lattice strains $\varepsilon(\varphi, hkl)$ [11]. In other words, with increasing pressure, for S to cross the zero value from positive to negative, the relative magnitudes of the elastic compliances along certain reflections must reverse (e.g., *111* [$\Gamma = 1/3$] to *200* [$\Gamma = 0$] for MgO); hence, the relative lattice strain magnitudes observed for these reflections should also reverse. In the situation where anisotropic crystallites are compacted as a Voigt solid under uniform differential stress, there should not be any systematic difference in lattice strains at one pressure, as can be seen in Fig. 1.

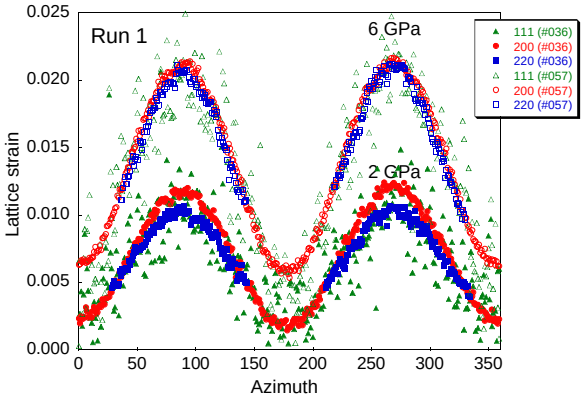

FIG. 1. Comparison of lattice strain at pressures of 2 and 6 GPa. The 111 reflection has the largest scatter due to its low intensity. The 220 *reflection could not be fully recorded on the CCD because of geometric constraint. Note the difference between 200 and 220 reflections. At 6 GPa, the strains of both reflections are identical, which indicates the anisotropy S is very close to zero.*

When an iso-stress model is assumed, the nonhydrostatic stress component can be written for *111* ($\Gamma = 1/3$), *200* ($\Gamma = 0$), and *220* ($\Gamma = 1/4$) peaks as follows:

$$\varepsilon_t(111) = (-t/3)[S_{44}/2], \quad (1)$$

$$\varepsilon_t(200) = (-t/3)[S_{11} - S_{12}], \text{ and} \quad (2)$$

$$\varepsilon_t(220) = (-t/3)[1/4(S_{11} - S_{12}) + 3/8\, S_{44}]. \quad (3)$$

By using any two of Eqs. (1)-(3), we can estimate *A*. However, our data for the *111* reflection are not as reliable as those for *200* and *220*, because of the low peak intensity and hence the large scatter in lattice strain determination. Here we compare *200* and *220* peaks; the apparent anisotropy *A* is given by

$$A = (3/4)(4\varepsilon_t(200)/[4\varepsilon_t(220) - \varepsilon_t(200)]). \quad (4)$$

The estimated apparent anisotropy *A* from *200* and *220* reflections is plotted in Fig. 2(a). When this is compared to differential stress data [7], we notice a correlation between the differential stress level and apparent elastic anisotropy. When the stress level is relatively low, the apparent anisotropy measured from diffraction is in good agreement with elastic anisotropy from ultrasonic measurements. However, once the sample reaches a certain stress level, the apparent anisotropy drops suddenly, offsetting the ultrasonic data. The apparent anisotropy factor observed in our data shows a nearly linear relationship with pressure, with a slope much steeper than that of elastic anisotropy [Fig. 2(b)]. Our data show excellent agreement with diffraction measurements in the DAC [9], which extends to much higher pressures. It is interesting to note the abrupt change in slope for the apparent anisotropy around 6 GPa in Merkel et al.'s DAC data [9]; beyond this point, *A* becomes more or less a constant.

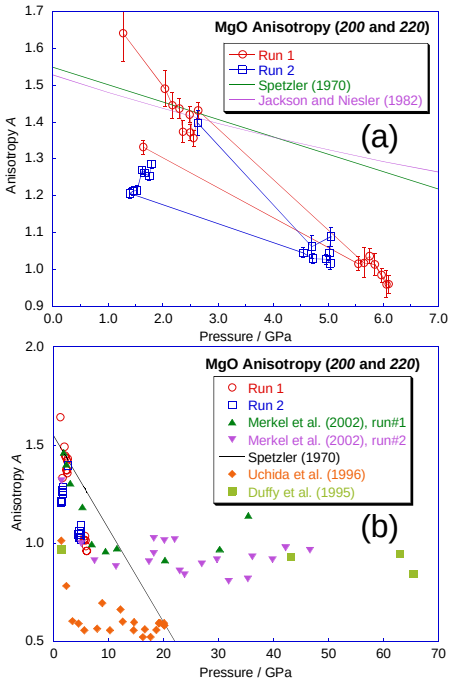

FIG. 2. Anisotropy A versus pressure from (a) this study and from (b) this study and previous diffraction studies. Up to a certain stress level, anisotropy is in good agreement with ultrasonic data. The anisotropy has offset from the adiabatic values under high differential stress level.

Figure 3 shows the relationship between the differential stress and each nonhydrostatic strain $\varepsilon_t(hkl)$, for comparison with Spetzler's ultrasonic data [1]. The slope of each line corresponds to the Young modulus for the given *hkl*. As the pressure increases, the slope becomes steeper according to the pressure dependence of the elastic constants. According to Spetzler [1], the difference in the slopes (i.e., elastic anisotropy) decreases with increasing pressure, so that all three slopes become identical at 11 GPa. During the first deformation cycle in run 1, the *200* and *220* peaks showed good agreement with ultrasonic data. In the second deformation cycle, both *111* and *220* data fell onto the *200* line ($A = 1$). In run 2, the high-pressure results showed again that all the data for *111*, *200*, and *220* fell on the *200* line predicted by the ultrasonic data. The low-pressure results showed some divergence, but the *220* data were still closer to the *200* data throughout the experiment than what the ultrasonic data predicted.

The discrepancy between our observation and the ultrasonic data, as seen in Figs. 2 and 3, is best explained by the yielding anisotropy of the crystallites in the bulk sample. According to Hulse et al. [12], the yield strength of single-crystal MgO is lowest in [100] at room temperature, with the [110](110) slip system being the dominating

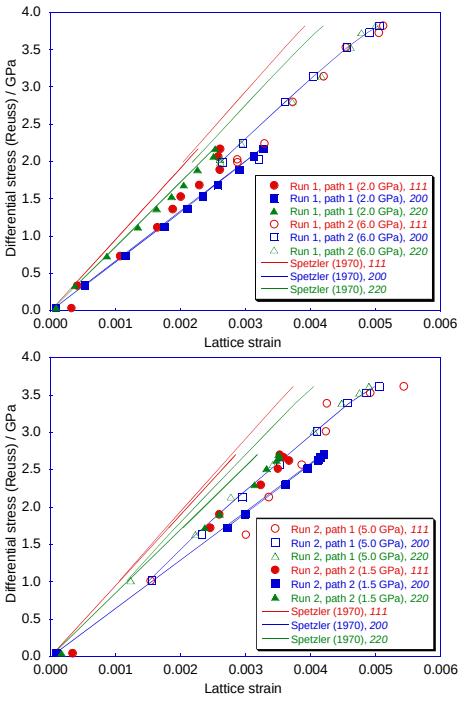

FIG. 3. Comparison of Young modulus for each peak. Solid lines show ultrasonic data [1]. Up to a certain stress level, the stress and strain relationship is identical to ultrasonic measurements, while all peaks shift toward strains of 200 peak under higher stress conditions. At high pressure, all strains are identical.

deformation mechanism. Figure 4 shows a representation of the differential stress-lattice strain relationship for Reuss and Voigt models at a certain pressure. We observe lattice strains and calculate differential stress by using known elastic constants under Reuss or Voigt model assumptions. At relatively low lattice strains (i.e., below point b_1 in Fig. 4), we are in the elastic regime and the stress-strain relation is linear. Thus, the diffraction data can be used to calculate a uniform differential stress t_1, and the resultant stress-strain relations are consistent with ultrasonic measurements. The first deformation cycle in run 1 shows this trend. However, as the differential stress levels increase to the point where the [100] crystallites reach yielding but the [111] and [110] crystallites do not, any differential stress level above the [100] yield strength must be supported by crystallites with other orientations (indicated by the kink in the *200* curve at t_2). At this point, the uniform differential stress assumption breaks down because of stress redistribution, and the Miller index dependence in the lattice strain rapidly disappears. Thus the iso-stress model underestimates differential stresses for crystallites with [111] and [110] directions. As the sample is further deformed, crystallites with [111] and [110] orientations

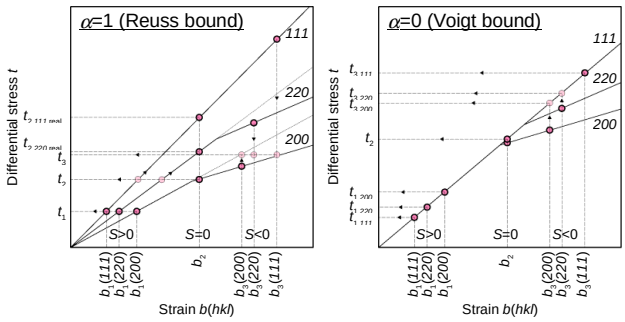

FIG. 4. Cartoon diagram of differential stress–lattice strain relationship for Reuss and Voigt models at a certain pressure. Stress is not observable but is obtained from strain(s) using elastic constants. At certain conditions, real stress could vary from the obtained value.

may sustain much higher stress, so the index dependence on the strains reverses, resulting in a reverse of the apparent anisotropy. When the [110] crystallites yield, the stress in the [111] crystallites is further enhanced (b_3 in Fig. 4). Since differential stresses are still calculated from the strains based on the elastic (linear) relationship, we tend to overestimate stress for *200* and underestimate stress for *111* and *220*. In the Voigt model, it is assumed that lattice strain is identical and thus a unique solution is obtained only from b_2. When the [100] crystallites reach yielding but the [111] and [110] crystallites do not, differential stress for the [100] crystallites is overestimated. When the [110] crystallites reach yielding, differential stress for the [110] crystallites is also overestimated. In any case, the Voigt model leads us to overestimate differential stress. The offset seen in Fig. 2(a) can be interpreted as slope change for *200* due to yielding and stress enhancement for *111* and *220*. If this is the case, an abrupt change in the apparent anisotropy [Eq. (4)] due to the yielding of [220] will occur. This is confirmed in previous data [5, 8, 9] [Fig. 2(b)].

Finally, this discussion focuses on measurements of elastic constants using the distortion of Debye ring (e.g., Refs. 13 and 9). Recently, the "radial diffraction" method has been widely used to estimate elastic constants using the DAC, by assuming a uniform differential stress level throughout the sample. However, our results indicate that one must be careful in controlling the differential stress level to within the elastic regime for these purposes. When the stress level is high and crystallites along certain directions begin to yield, the elastic constants thus obtained may be in error.

Acknowledgments

We thank N. Lazarz, F. Sopron, M. Jagger, G. Shen, M. Newville, P. Eng, J. Pluth, P. Murray, and C. Pullins for their valuable contributions. To convert 2-D diffraction data into "cake" form, the program FIT2D was used. We express

our thanks to A. Hammersley and the European-Synthrotron Radiation Facility (ESRF) personnel for the public use of FIT2D. We thank W. Durham for use of the D-DIA. We also thank S. Merkel for discussion. Work performed at GSECARS is supported by the National Science Foundation (Earth Sciences), U.S. Department of Energy (DOE, Geosciences), W.M. Keck Foundation, and U.S. Department of Agriculture. Use of the APS was supported by the DOE Office of Science, Office of Basic Energy Sciences, under Contract No. W-31-109-ENG-38.

References

[1] H. Spetzler, J. Geophys. Res. **75**, 2073-2087 (1970).
[2] G. Chen, R.C. Liebermann, and D.J. Weidner, Science **280**, 1913-1916 (1998).
[3] I. Jackson and H. Niesler, in *High Pressure Research in Geophysics*, edited by S. Akimoto and M.H. Manghnani (D. Reidel Publishing Co., copublished with Center for Academic Publications, Tokyo, Japan, 1982), pp. 93-113.
[4] S.V. Sinogeikin and J.D. Bass, Phys. Rev. B **59**, 14141-14144 (1999).
[5] T. Uchida, T. Yagi, K. Oguri, and N. Funamori, Rev. High Pressure Sci. Technol. **7**, 269-271 (1998).
[6] W. Wang, W.B. Durham, I.C. Getting, and D.J. Weidner, Rev. Sci. Instrum. **74**, 3002-3011 (2003).
[7] T. Uchida, Y. Wang, M. Rivers, and S. Sutton, "Differential stress in MgO measured in the deformation-DIA by using high-resolution monochromatic diffraction," *Advanced Photon Source Activity Report 2002*, ANL-03/21 (Argonne National Laboratory, Argonne, IL, December 2003).
[8] T.S. Duffy, R.J. Hemley, and H.K. Mao, Phys. Rev. Lett. **74**, 1371-1374 (1995).
[9] S. Merkel, H.R. Wenk, J. Shu, G. Shen, P. Gillet, H.K. Mao, and R.J. Hemley, J. Geophys. Res. **107** (11), 2271 (2002).
[10] A.K. Singh, J. Appl. Phys. **73**, 4278-4286 (1993).
[11] N. Funamori, T. Yagi, and T. Uchida, J. Appl. Phys. **75**, 4327-4331 (1994).
[12] C.O. Hulse, S.M. Copley, and J.A. Pask, J. Am. Ceram. Soc. **46**, 317-323 (1963).
[13] H.K. Mao, J. Shu. G. Shen, R.J. Hemley, B. Li, and A.K. Singh, Nature **396**, 741-743 (1998).